International Journal of Bio-Inorganic Hybrid Nanomaterials

Synthesis and Structural Characterization of Bi_2O_3 Loaded on the MCM-41 and Study of Its Photocatalytic Performance in Degradation of Methylene Blue

Shankar Lal Gargh[1], Majid Mozaffari[2], Mirabdullah Seyed Sadjadi[3]*

[1] Research Journal of BioTechnology, Sector AG/80, Scheme no.54, A.B.Road, Indore, India
[2] Department of chemistry, Shahrood Branch, Islamic Azad University, Shahrood, Iran
[3] Department of chemistry, Science and Research Branch, Islamic Azad University, Tehran, Iran

ABSTRACT

In this work, we report synthesis and characterization of Bi_2O_3 nanoparticles loaded on mesoporous MCM-41 nanoparticles by a simple solid-state dispersion (SSD) method. Monoclinic bismuth oxide nanoparticles were prepared by polyacrylamide gel method and used as loading materials on the prepared mesoporous MCM-41 as a supporting material. Fourier transform infrared spectroscopy (FT-IR), X-ray powder diffraction (XRD) and transmission electron microscopy (TEM) and the high resolution transmission electron microscopy (HRTEM) were used to study the structural and morphological characteristic of the prepared nanocomposite samples. Photocatalytic performance of the prepared samples was finally evaluated by degradation of methylene blue under irradiation of UV and visible light. The results revealed that, Bi_2O_3 loaded on nanosize MCM-41 has higher photocatalytic activity than that of pure starting Bi_2O_3 nanoparticles.

Keyword: Mesoporous MCM-41; Solid-state dispersion method; Bi_2O_3 nanoparticles; Methylene blue degradation; Nanocomposite.

1. INTRODUCTION

Photocatalysis is a "green" technique offers a potential for complete elimination of the toxic chemicals in the environment through its efficiency and broad applicability in energy reforming technologies [1]. So, photocatalytic degradation of organic pollutants that influence life-form human health continues to attract interest as a method to mitigate their impact on the environment. Many semiconductor oxides like TiO_2, Fe_2O_3, ZnO, ZrO_2, Nb_2O_5, WO_3, Bi_2O_3, SnO_2, etc. have been

(*) Corresponding Author - e-mail: m.s.sadjad@gmail.com

Int. J. Bio-Inorg. Hybd. Nanomat., Vol. 1, No. 3 (2012), 183-192

Lal Gargh Sh et al

used as photocatalysts in the wastewater treatment of organic synthesis and water splitting reactions [1-5]. Since, illumination of the semiconductors with a light in an appropriate wavelength makes them a powerful oxidant to convert most of the organic molecules into carbon dioxide and water. In this process, excitation of the photocatalysts produce holes and electrons in the valence and conduction bands and the photo-generated holes have a strong oxidation power and are widely studied for environmental cleaning.

Recent studies have demonstrated that, hetero-geneous photocatalysis using TiO_2 as photocatalyst appears as the most emerging destructive technology [6]. But, large band gap energy (3.2 eV) for anatase TiO_2 (excitation wavelength < 387.5 nm), limits its practical application under the condition of natural solar light [7]. In order to meet requirement of the future environmental and energy technologies, it is necessary to develop more efficient and stable visible-light photocatalysts. Therefore, visible-light-driven photocatalysts by using semiconductors have attracted much interest because visible light occupies the main part of the solar spectrum and can be easily utilized [8-10]. Traditional visible-light photocatalysts are either unstable under solar light illumination (e.g., CdS, CdSe) [11] or have low activity (e.g., Fe_2O_3) [12]. While, Bismuth oxide is an important metal-oxide semiconductor with a direct band gap of 2.8 eV and it can be excited by visible light [13, 14]. Bessekhouad et al. applied Bi_2O_3 semiconductor to degrade orange II pollutant in water under visible light. But, efficiency of the photocatalytic degradation by Bi_2O_3 should be further improved in order to meet the requirements of environmental protection [15]. It is also well known that the light-generated charge carriers in micron sized semiconductors cannot be efficiently transfered to the surface and are lost due to recombination, which results in low solar energy conversion efficiency. While, the grain size being reduced from micron- to nanosized scale, can dramatically reduces opportunities for recombination effect [16]. Therefore, preparation of nanosized Bi_2O_3 particles seems to be an appropriate candidate to improve

photocatalytic activity. Furthermore, it has been recently reported that mesoporous (MCM-41), microporous (β-zeolite) and pillared structure (montmorillonite) supported TiO_2 exhibits a good photodegradation efficiency of orange II under UV light [17]. Support materials with high surface area and good acidic properties adsorb organic pollutants in vicinity to the catalyst active sites and results in enhanced photocatalytic degradation rate. Photocatalytic efficiency is also improved by decreasing the electron-hole recombination possibility, facilitating the interfacial charge transfer from the surface of the photocatalyst to the substrate. Accordingly, nano-sized MCM-41 was firstly synthesized in this work and used as a support to disperse Bi_2O_3 photocatalyst. Photocatalytic activity performance of prepared nanocomposite samples in degradation of methylene blue under irradiation of UV and visible light in comparison to Bi_2O_3 will be reported.

2. EXPERIMENTAL

2.1. Preparation of mesoporous MCM-41 nanoparticles

Sodium silicate solution (25.5 - 28.5 wt% SiO_2 and 7.5 - 8.5 wt% Na_2O, MERK), cetyltrimethylammonium bromide (CTAB, 99%, BDH), acetic acid glacial (100%, analytical regent grade), $Bi(NO_3)_3 \cdot 5H_2O$ (Aldrich), HNO_3 (Fischer), acrylamide (99.0%), N,Nó-methylenebisacrylamide (99.0%), ammonium persulphate and ammonium hydroxide solution used in this work, all were of analytical grade. Mesoporous MCM-41 silica was synthesized using a gel mixture with a composition of $4SiO_2$: $1CTAB$: $250H_2O$ according to the reported procedure [18]. For this purpose, to a required amount of the CTAB dissolved in an appropriate amount of water, sodium silicate solution was slowly added and stirred for 30 min. The pH of the mixture was then adjusted to 10 by adding acetic acid and the gel obtained was put in a polypropylene bottle and refluxed at 100°C for 24 hrs. After cooling and adjusting the pH at 10

Lal Gargh Sh et al

Int. J. Bio-Inorg. Hybd. Nanomat., Vol. 1, No. 3 (2012), 183-192

with acetic acid, the mixture was refluxed again for 24 hrs at 100°C. The pH adjustment and subsequently heating operations were repeated several times for 5 days and the resulting gel was filtered and washed with distilled water and dried in an oven to obtain a white mesoporous MCM-41 nanopowders.

2.2. Preparation of Bi2O3 nanoparticles

Bi_2O_3 nanoparticles were prepared by a modified polyacrylamide-gel method which is described in the literature [19]. Required amounts of acrylamide monomer, N,N'-methylenebisacrylamide as lattice reagent or polymer-network and ammonium persulphate as catalyst were added in turn to a dilute nitric acid solution of bismuth nitrate (Bi^{3+}: 0.05 mol/l). The mass ratio between monomer and lattice reagent was 3:1 respectively. Ammonium hydroxide solution was then added into the mixing solution until to the pH value reached 9. The mixture was stirred in water bath at room temperature and turned into the gel at 60°C by slow increase of the water bath temperature, and calcined subsequently in flowing air at 300°C for 6h by increasing the temperature at the range of 5°C/ min to obtain a light yellow powder.

2.3. Preparation of Bi₂O₃- MCM-41

Bi_2O_3/MCM-41 nanocomposite systems were prepared via a simple solid-state dispersion (SSD) method by mixing different amounts of Bi_2O_3 nanoparticles (5, 10 and 15 wt %) with a required mesoporous MCM-41 nanoparticles in a minimum quantity of n-butyl alcohol. The mixtures were then dried in an oven at 100°C for overnight and named BM-1, BM-2 and BM-3, respectively.

2.4. Structural characterization

Structural characterization of the samples were performed by using powder X-ray diffraction patterns recorded on a Bruker Advance D8 Diffractometer using Cu K_α radiation (λ=0.154 nm). The FT-IR spectra were recorded using a Perkin Elmer FT-IR spectrometer by employing KBr pellet technique. The TEM measurement was performed on a Philips EM208 microscope operated at 100 kV. The HRTEM measurement was performed on a Philips CM 200 FEG/HRTEM operated at 200 kV.

2.5. Measurement of photocatalytic activity

Photocatalytic activity of the prepared samples was evaluated via degradation of Methylene Blue (MB) as a contaminant model compound. The photoreaction were carried out in a 100 ml Pyrex vessel which positioned at 10 cm distance under a high pressure mercury UV lamp (125 W, 254-365 nm) and a Blue LED light bulb (1W, 400-500 nm) as UV and visible-light sources respectively. In a typical experiment, 0.1 g of the samples in 100 ml of MB solution (6.74×10^{-6} M) were sonicated for 10 min and stirred magnetically for 30 min in darkness to reach adsorption equilibrium. The lamps were then switched on to initiate illumination of the samples. During illumination, the suspensions were stirred for 600 rpm at 25°C. The residual MB in the solutions was analyzed by checking the absorbance at 664 nm with a UV-Vis spectrophotometer (Perkin Elmer Lambda 25).

3. RESULTS AND DISCUSSION

3.1. Structural characterization

Figure 1A represents low angle X-ray diffraction patterns of calcined MCM-41(a) and as prepared nanocomposite samples of BM-1(b), BM-2(c) and BM-3(d). In this figure, the very intense peak appeared at low angle (2θ=2.55) is assigned to reflections at (100) and two other additional picks in low intensities at (110) and (200) reflections indicating regular pore structure of the MCM-41, is attributed to the quasi-two-dimensional hexagonal lattice structure of MCM-41 [20]. This figure shows also that on dispersing Bi_2O_3 over MCM-41, a decrease in the peak intensity of the characteristic (100) plan is predominant while, at higher Bi_2O_3 loaded samples, the peaks of (110) and (200) planes tend to merge with the base line. Decrease of peck intensity can be attributed to the pores filling effects that reduce the scattering contrast between the pores and the framework of MCM- 41sample.
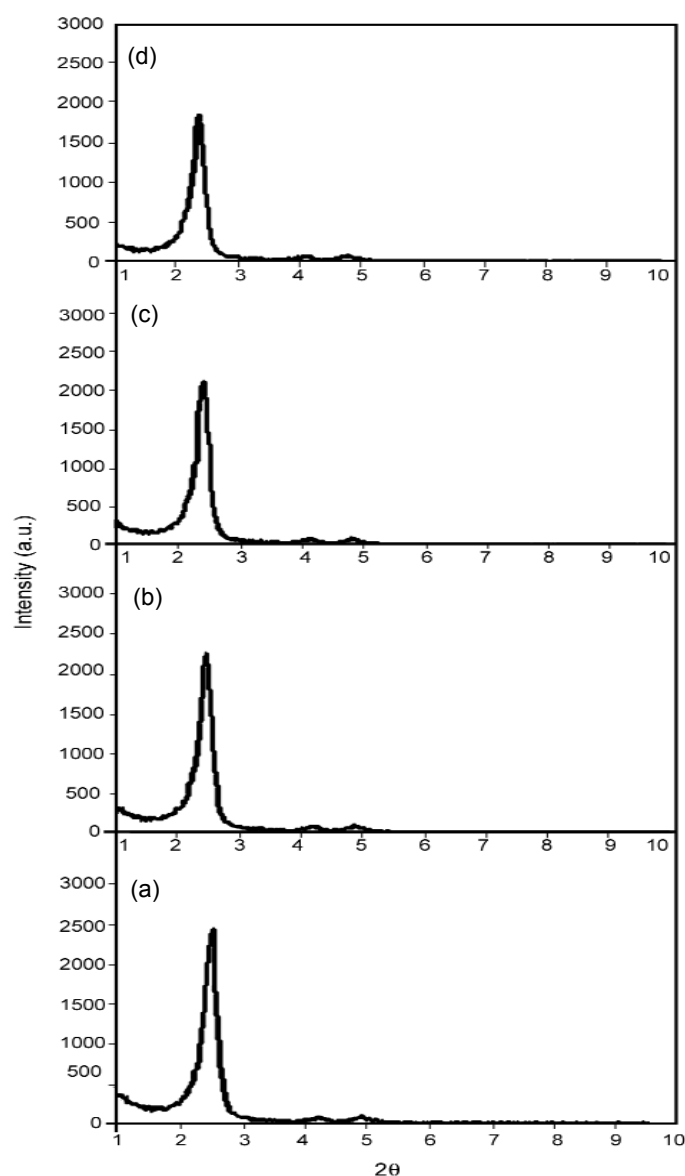
Int. J. Bio-Inorg. Hybd. Nanomat., Vol. 1, No. 3 (2012), 183-192

Lal Gargh Sh et al

Figure 1A: *Low angle XRD patterns of: (a) MCM-41; (b) BM-1; (c) BM-2; (d) BM-3.*

Figure 1B (a, b, c) shows the wide angle X-ray patterns (2θ=20-60°) of as prepared BM-1, BM-2 and BM-3 nanocomposites respectively. In this figure, the characteristic peaks appeared at 2θ=26.94, 2θ=27.40 and 2θ=33.25 confirm the presence of Bi_2O_3 phase in Bi_2O_3/MCM-41 nanocomposites. Note that Bi2O3 has four polymorphic forms with distinct crystalline structures and physical (electrical, optical, etc.) characteristics [21]: α-Bi_2O_3 which is stable at low temperature and reported to be in monoclinic form; δ-Bi_2O_3 that is stable polymorphic cubic form at high temperature [22, 23] and two other high-temperature metastable polymorphous phases known as tetragonal β-Bi_2O_3 and γ-Bi_2O_3 [23]. In general, preparation of the different forms of Bi_2O_3 depends strongly to the synthesis method and at the present case, all the diffraction peaks can be assigned to bismuth oxide, crystallized in monoclinic form corresponding to JCPDS files no.
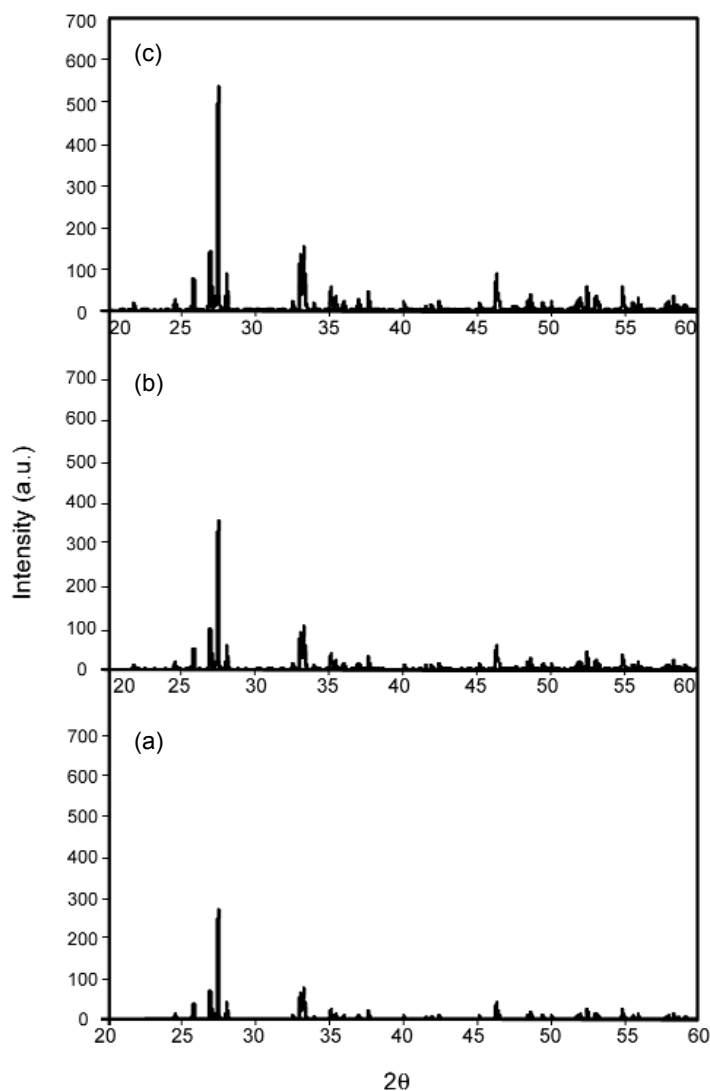
Figure 1B: *wide angle XRD patterns of: (a) BM-1; (b) BM-2; (c) BM-3.*

41-1449. The average crystalline sizes were determined from X-ray diffraction patterns according to the Scherrer's equation [24]:

$$D = k\lambda / \beta \cos \theta$$

Where D is the average grain size, k is a constant equal to 0.9, λ is X-ray wavelength equal to 0.15406 nm and β is the half-peak width. It was found that the average crystalline sizes of MCM-41, BM-1, and BM-2 and BM-3 nanopowders using Scherrer's equation were around 46 nm.

Figure 2 (a, b, c and d) shows the FT-IR spectra of MCM-41, α-Bi_2O_3 and as prepared BM-1 and BM-2 samples. In the spectrum of raw MCM-41 (Figure 2a), the broad intense double bands appeared at about 1000-1290 cm^{-1} is due to asymmetric stretching vibrations of Si-O-Si bridges and the absorption bands observed at 467 and 812 cm^{-1} are assigned to the asymmetric and symmetric Si-O stretching vibrations [25, 26].

In the spectrum of α-Bi_2O_3 (Figure 2b), the absorption bands at 510 and 540 cm^{-1} are specific to the vibrations of Bi-O bonds in BiO_6 octahedral

Int. J. Bio-Inorg. Hybd. Nanomat., Vol. 1, No. 3 (2012), 183-192
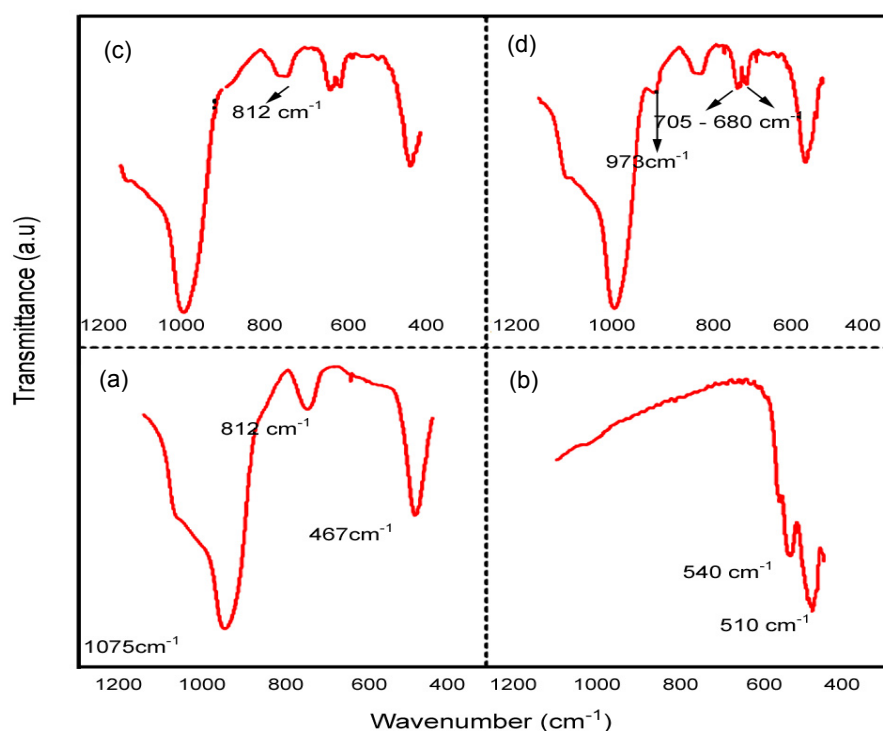
Lal Gargh Sh et al

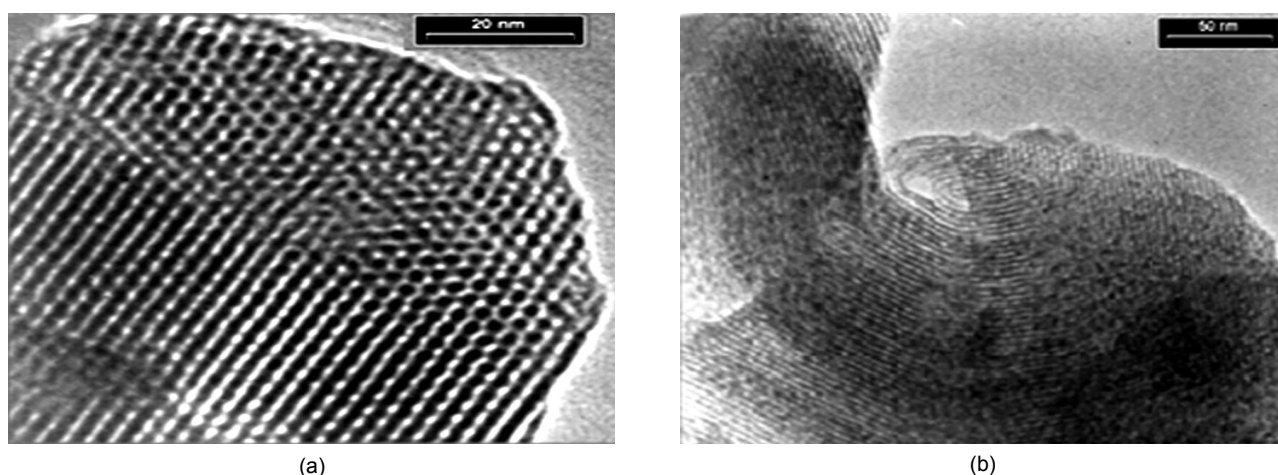**Figure 2:** *FT-IR spectra of: (a) MCM-41 (b) Bi2O3); (c) BM-2: (d) BM3.*

Figure 3: *TEM images of (a) BM-1, (b) BM-2.*

units and on the dispersed Bi_2O_3 over MCM-41 samples (Figure 2 (c, d)), and the two new absorption bands appeared at about 680-705 cm^{-1} and 973 cm^{-1}, in comparison with the raw MCM-41 spectra and in similarity to the results reported elsewhere can be ascribed to the stretching vibration of Bi-O and Bi-O-Si bridges [27, 28] respectively. Figure 3 (a, b) shows TEM images of BM-1 and BM-2 nanoparticles. The ordered hexagonal pore arrangements of these two samples were clearly visible and can be estimated to be in the range of 2.6-3 nm with a thick wall about 1 nm.

The images of TEM indicated that the nanoparticles sizes were similar and fairly small, and the average particle sizes as we reported in this work were almost 40-50 nm in diameter.

3.2. Photoreduction of methylene blue

Methylene blue absorbs the light in the visible region (550-700 nm) with a maximum absorption at 664 nm without any photocatalysis. MB has been reported to be a photobleached and photodegradable material under visible light irradiation [29]. In order to clarify how the prepared Bi_2O_3/MCM-41 nanocomposites behave as photocatalyst for the degradation of MB, the blue LED with the wavelength of 400-500 nm is adapted as the light source to evade the self-photobleaching of MB in the visible light region since, the MB molecules may be photosensitized by the visible light around 664 nm to reduce intensity of the characteristic adsorption peaks. Figure 4A represents the photo degradation of MB vs. irradiation time for the samples Bi_2O_3 (a); BM-1(b); BM-2 (c) and BM-3(d) under blue LED light irradiation. A simple reference to this MB degradations data shows that the maximum photocatalytic activity has occurred for the samples containing 5% of Bi_2O_3 (BM-2).
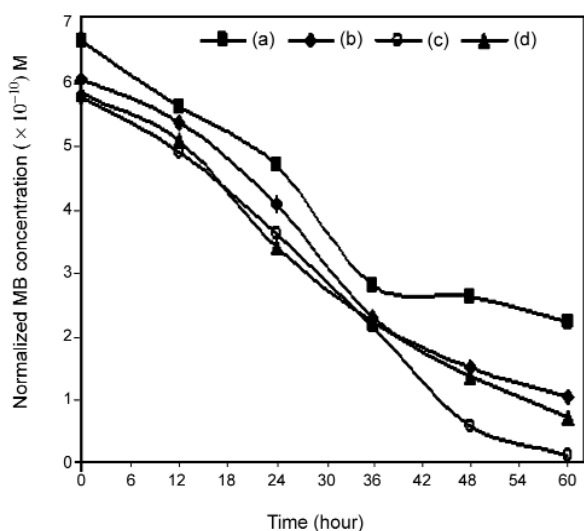
Figure 4A: *Photodegradation of MB on: (a) Bi_2O_3 (b) BM-1(c) BM-2 (d) BM-3 under visible light irradiation.*

Figure 4B shows that, the same photocatalytic activity has been observed for the BM-2 sample for MB degradation vs. irradiation time under UV light irradiation. Obtained data in this case more clearly shows efficient MB degradation for the samples BM-2.
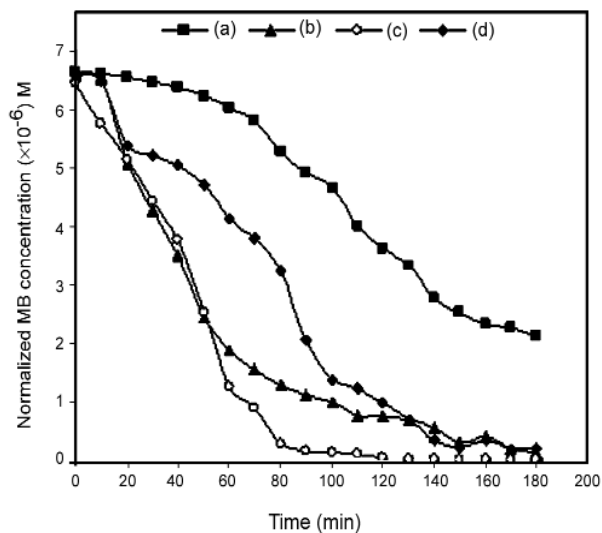
Figure 4B: *photoreduction of MB over (a) Bi_2O_3 (b) BM-1(c) BM-2 (d) BM-3 under UV light irradiation.*

Figure 5A illustrates the photodegradation of MB under blue light LED irradiation in an interval time of 12 h for the samples of BM-2. It was found that the decolorization process of MB proceeds by increasing irradiation time, and the normalized con centration of MB solution decreases. A faster decrease in intensity of absorption at 664 nm (Figure 5B) suggests that the chromophore responsible for characteristic color of MB is breaking down as the irradiation time increases. The small blue shift which could be observed is due to the formation of the demethylated dyes, as were reported by Chihiro Yogi et al. [30]. We note that, the shoulder around 610 nm in the MB aqueous solution is well known to come from a vibrational component (at ∼ 610 nm) of the MB monomer electronic band and an absorption peak (at ∼ 605 nm) of the MB dimmer [31]. The intensity of this shoulder around 610 nm varies in resemblance to the maximum characteristic peak at 664 nm, and no blue shift was found under the blue LED light irradiation. It means that only photodegradation of MB is occurred under blue LED light irradiation.
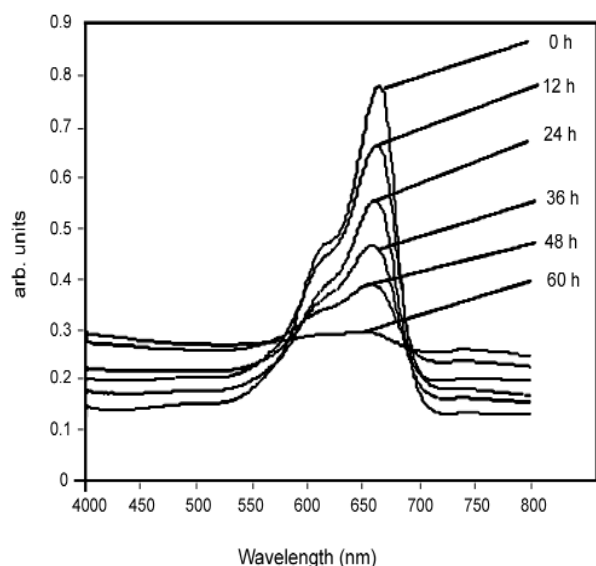
Figure 5A: *Photodegradation of MB on the BM-2 nanocomposite under visible light irradiation versus time.*
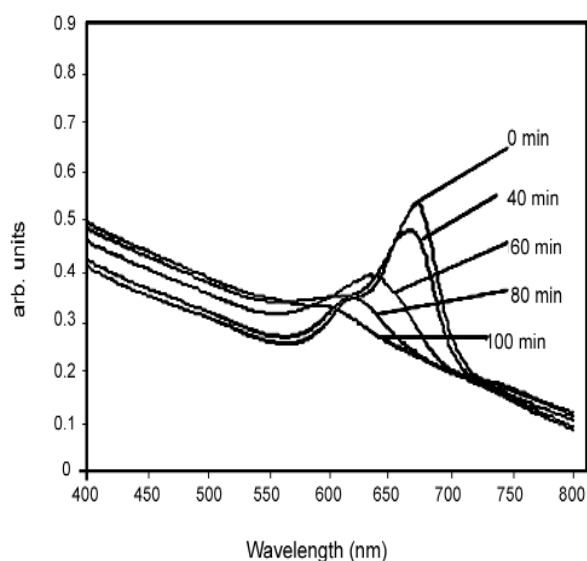

Figurer 5B: *Photodegradation of MB on the BM-2 nanocomposite under UV irradiation versus time.*

The results obtained from Figures 4 and 5 show that the photoactivity of the Bi_2O_3 loaded MCM-41 nanocomposites is considerably dependent on the doped Bi^{+3} amounts. The maximum amount of the MB degradation is found for Bi^{+3} doping of 10% (BM-2). In monoclinic Bi^{+3} semiconductors, the potential of the valence band of Bi-6s is more negative than that of O-2p [32]. The hybrid

Bi-6s - O-2p is believed to be suitable for the appropriate band gap of monoclinic Bi_2O_3, which results that monoclinic Bi_2O_3 can be excited by visible light. The bottom of the conduction band is formed mainly by the Bi-6p orbital with a small contribution from O-2p. The band structure indicates that charge transfer upon photoexcitation occurs from the hybrid orbital of O-2p and Bi-6s to the empty Bi-6p orbital. Mesoporous MCM-41 with high surface area adsorb organic pollutants in vicinity to the active sites for dye-semiconductor interactions that results in enhanced photocatalytic degradation rate. Furthermore the electron-rich MCM-41 surface functions as a whole scavenger that improved the photocatalytic efficiency by decreasing the electron-hole recombination, facilitating the interfacialcharge transfer from the surface of the photocatalyst to the substrate. For getting accurate kinetic data, kinetic experiment was also carried out to assure the adsorption equilibrium reached. It was well-known that photocatalytic oxidation of organic pollutants follows Langmuir-Hinshelwood kinetics [33-36]. This kind of reaction can be represented as follows:

$$-\frac{dc}{dt} = kt$$

It can be integrated as follows:

$$kt = Ln\frac{Co}{C}$$

Where C_o / C is the initial concentration of the MB solution to the reached molarity of the solute and k is the rate constant. The apparent rate constants for the different photocatalysts prepared in this work were calculated and listed in Table 1.

It can be clearly seen that the addition of Bi_2O_3, significantly improve the photodegradation activity of the MCM-41 under UV and visible irradiations. The catalyst BM-2 has the highest rate constant of 0.0610 min^{-1} under UV irradiation. While the highest rate constant for the same BM-2 catalyst observed under visible irradiation was 0.0539 h^{-1}. These observed values are much higher than that of Bi_2O_3 to be 0.0056 min^{-1} and 0.0196 h^{-1} respectively under UV and visible irradiations.

Lal Gargh Sh et al

Int. J. Bio-Inorg. Hybd. Nanomat., Vol. 1, No. 3 (2012), 183-192

Table 1: *The rate constant for degradation of MB over Bi2O3 and Bi2O3 loaded mesoporous MCM-41 under UV and visible light irradiation.*

Catalyst	k (min^{-1}) UV	k (h^{-1}) Visible light
Bi_2O_3	0.0056	0.0196
BM-1	0.0191	0.0301
BM-2	0.0610	0.0539
BM-3	0.0183	0.0344

4. CONCLUSIONS

In summary:

• Bi_2O_3 nanoparticles were prepared by a modified polyacrylamide-gel method and used to prepare Bi_2O_3 / MCM- 41 nanocomposites by a simple solid-state dispersion (SSD) method.

• Characterization of as prepared Bi_2O_3 nanoparticles on mesoporous MCM-41 nanocomposites was performed by XRD, FTIR and TEM.

• Photocatalytic activity of as prepared nanocomposite have carried out and the results showed that nanosized Bi_2O_3 supported on mesoporous MCM-41, comparing to the pure Bi_2O_3 is a very active photocatalyst for degradation of methylene blue.

• Enhanced photocatalytic activity of as prepared nanocomposites attributed to the high surface area of MCM-41 substrate which adsorb organic pollutants in vicinity to the active sites of dye-semiconductor interactions and the electron-rich MCM-41 surface functions as a hole scavenger that improve the photocatalytic efficiency of the nanosized Bi_2O_3 by decreasing electron-hole recombination and facilitating interfacial charge transfer from the surface of the photocatalyst to the substrate.

REFERENCES

1. Hoffman M.R., Martin S.T., Choi W., Bahnem-ann D.W., *Chem. Rev.*, **95**(1995), 69-96.

2. Carp O., Huisman C.L., Reller A., *Prog. Solid State Chem.*, **32**(2004), 33-177.

3. Subba Rao K.V., Srinivas B., Subrahmanyam M., *Photo/Electrochem. Photobiol. Environ. Energy Fuel*, (2004), 31-89.

4. Krishna Reddy J., Lalitha K., Durga Kumari V., Subrahmanyam M., *Catal. Lett.*, **121**(2008), 131.

5. Ratnamala A., Suresh G., Durga kumari V., Subrahmanyam M., *Mater. Chem. Phys.*, **110**(2008), 176.

6. Konstantinou K., Albanis T.A., Appl. *Catal. B: Environ.* **49**(2004), 1-14.

7. Wang J., Uma S., Klabunde K.J., *Appl. Catal. B: Environ.* **48**(2004), 151-154.

8. Fox M.A., Dulay M.T., *Chem. Rev.*, **93**(1993), 341.

9. Fujishima A., Rao T.N., Tryk D.A., *J. Photochem. Photobiol. C: Photochem. Rev.*, **1**(2000), 1.

10. Yu J.C., Yu J.G., Ho W.K., Jiang Z.T., Zhang L.Z., *Chem. Mater.*, **14**(2002), 808.

11. De G.C., Roy A.M., Bhattacharya S.S., *Int. J. Hydrogen Energy*, **21**(1996), 19.

12. Hwang D.W., Kim J., Park T.J., Lee J.S., *Catal. Lett.*, **80**(2002), 53.

13. Maruthamuthu P., Gurunathan K., Subramanian E., *Int. J. Hydrogen Energy*, **19**(1994), 889.

14. Gurunathan K., Int. *J. Hydrogen Energy*, **29**(2004), 933.

15. Bessekhouad Y., Robert D., Weber J.V., *Catal. Today*, **101**(2005), 315.

16. Zhang L., Lin J., Chen Z., Tang Y., Yu Y., *Appl. Catal. A: Gen.*, **299**(2006), 292.

17. Bhattacharyya A., Kawi S., Ray M.B., *Catal. Today*, **98**(2004), 431- 439.

18. Sadjadi M.S., Mozaffari M., Enhessari M., Zare K., *Superlattices Microstruct*, **47**(2010), 685-694.

19. Pan C., Li X., Wang F., Wang L., *Ceram. Int.*, **34**(2008), 439- 441.

20. Kresge C.T., Leonowicz M.E., Roth W.J., Vartuli J.C., Beck J.S., *Nature*, **359**(1992), 710-712.

21. Leontie L., Caraman M., Delibas M., Rusu G.I., *Mater. Res. Bull.*, **36**(2001), 1629.

22. Irmawati R., Noorfarizan Nasriah M.N., Taufiq-Yap Y.H., Abdul Hamid S.B., *Catal. Today*, **93**(2004), 701.

23. Monnereau O., Tortet L., Llewellyn P., Rouquerol F., Vacquier G., *Solid State Ionics*, **157**(2003), 163.

24. Cullity B.D., *Elements of X-ray Diffraction*, 2nd ed., Eddison-Weiley, Publishing Company Inc. Reading, MA 1978.

25. Romero A.A., Alba M.D., Zhou W., Klinowski J., *J. Phys. Chem. B*, **101**(1997), 5294-5300.

26. Takahashi R., Sato S., Sodesawa T., Kawakita M., Ogura K., *J. Phys. Chem. B*, **104**(2000), 12184-12191.

27. Li J., Liu S., He Y., Wang J., *Microporous and Mesoporous Materials*, **115**(2008), 416-425.

28. Sadjadi M.S., Farhadyar N., Zare K., *Superlattices Microstruct.*, **46**(2009), 266-271.

29. Romero A.A., Alba M.D., Zhou W., Klinowski J., *J. Phys. Chem. B*, **101**(1997), 5294-5300.

30. Takahashi R., Sato S., Sodesawa T., Kawakita M., Ogura K., *J. Phys. Chem. B*, **104**(2000), 12184-12191.

31. Mills A., Wang J., *J. Photochem. Photobiol. A*, **127**(1999), 123-134.

32. Yogi C., Kojima K., Wada N., Tokumoto H., Takai T., Mizoguchi T., Tamiaki H., *Thin Solid Films*, **516**(2008), 5881-5884.

33. Bergmann K., O'Konski C.T., *J. Phys. Chem.*, **67**(1963), 2169-2177.

34. Kudo A., Omori K., Kato H., *J. Am. Chem. Soc.*, **121**(1999), 11459.

35. Li Y.Z., Kim S.J., *J. Phys. Chem. B*, **109**(2005), 12309.

36. Hong S.S., Lee M.S., Park S.S., Lee G.D., *Catal. Today*, **87**(2003), 99.